

Supporting Information for:

Octacyanom Metallate qubit candidates

Tyler J. Pearson,[†] Daniel W. Laorenza,[†] Matthew D. Krzyaniak,^{†,§} Michael R.
Wasielewski^{†,§} and Danna E. Freedman^{*,†}

*[†] Department of Chemistry and [§] Argonne-Northwestern Solar Energy Research
Center, Northwestern University, 2145 Sheridan Road, Evanston, Illinois 60208-
3113, United States*

Dalton Trans.

Table of Contents

Experimental Details	S3
Table S1 Echo-detected EPR spectrum fit parameters	S6
Table S2 Saturation recovery curve fit parameters for 1 w/ spec. diffus. in PrCN	S7
Table S3 Saturation recovery curve fit parameters for 1 w/o spec. diffus. in PrCN	S7
Table S4 Saturation recovery curve fit parameters for 1 w/ spec. diffus. in DMF/tol	S9
Table S5 Saturation recovery curve fit parameters for 1 w/o spec. diffus. in DMF/tol	S10
Table S6 Saturation recovery curve fit parameters for 2 w/ spec. diffus. in PrCN	S11
Table S7 Saturation recovery curve fit parameters for 2 w/o spec. diffus. in PrCN	S12
Table S8 Saturation recovery curve fit parameters for 2 w/ spec. diffus. in DMF/tol	S13
Table S9 Saturation recovery curve fit parameters for 2 w/o spec. diffus. in DMF/tol	S14
Table S10 T_1 temperature dependence fit parameters w/ spec. diffus.	S15
Table S11 T_1 temperature dependence fit parameters w/o spec. diffus.	S16
Table S12 T_2 temperature dependence fit parameters	S17
Table S13 T_2 temperature dependence fit parameters	S18
Table S14 T_2 temperature dependence fit parameters	S19
Table S15 T_2 temperature dependence fit parameters	S20
Figure S1 Echo-detected EPR spectra	S21
Figure S2 Saturation recovery curves and fits for 1 in PrCN	S22
Figure S3 Saturation recovery curves and fits for 1 in DMF/tol	S23
Figure S4 Saturation recovery curves and fits for 2 in PrCN	S24
Figure S5 Saturation recovery curves and fits for 2 in DMF/tol	S25
Figure S6 Monoexponential vs. spectral diffusion T_1 values	S26
Figure S7 Temperature dependence of T_1 and fits for 1	S27
Figure S8 Temperature dependence of T_1 and fits for 2	S28
Figure S9 Temperature dependence of T_2 for 1	S29
Figure S10 Temperature dependence of T_2 for 2	S30
Figure S11 Demonstrations of Rabi oscillations	S31
References	S32

Experimental Details

General Considerations. Unless otherwise noted, all compounds were purchased from commercial sources and used without further purification. We synthesised both **1** and **2** via literature methods.¹ All samples were prepared under anaerobic conditions in a dinitrogen glovebox to prevent contamination by dioxygen.

EPR Measurements. We acquired solution phase data on multiple samples of both **1** and **2** to ensure reproducibility. We measured samples in two solvent systems: dry, deoxygenated butyronitrile, or 40 vol% dimethylformamide/toluene. We ensured that all samples had concentrations below 1 mM to limit dipolar contributions.² Here, we report a sample of **1** in 0.5 mM in PrCN and 0.5 mM in 40 vol% DMF/toluene, and a sample of **2** in 0.5 mM in DMF/toluene and 0.5 mM butyronitrile. All samples were prepared in 4 mm OD quartz EPR tubes (Wilmad Labglass) and, depending on the time between preparation and measurement, either flame sealed under high vacuum or flash frozen in liquid nitrogen under an atmosphere of N₂ to prevent contamination of the solvent glass by O₂. For data collection on the same sample over multiple days, samples were stored in liquid N₂ between measurements to prevent decomposition. We acquired EPR data at X-band (~9.5 GHz) on all samples using a Bruker E580 X-band spectrometer equipped with a 5 mm split ring resonator (Bruker ER4118X-MS5) and a 1 kW TWT amplifier (Applied Systems Engineering) at Northwestern University. For all pulsed measurements, the resonator was overcoupled to prevent ringdown following the application of the microwave pulses. Temperature was controlled using an Oxford Instruments Mercury iTC cryostat. *T*₁ data were collected on the most intense central resonance in the echo-detected EPR spectrum (Figure S1) using a saturation recovery sequence with a 4- or 8-step phase cycle. This sequence consisted of eight 20 ns picket fence pulses to saturate the transition followed by a delay (*T*), and a detection sequence $\pi/2 - \tau - \pi - \tau - \text{echo}$ in which $\pi/2 = 16$ ns, $\pi = 32$ ns, and $\tau = 240$ ns. *T* was incremented from a starting value of 100 ns.

We phased the *T*₁ data by maximization of the sum of squares of the data points in the real component of the spectrum, normalised them such that the data spanned the intensity range between 0 and 1, and then fit the data using a monoexponential function of the form

$$I(t) = -A(e^{-t/T_1} - d - 1)$$

where *I* is the normalised echo intensity, *A* and *d* are normalization coefficients (approximately 1 and 0 respectively), and *t* is the delay time (s). Data were also fit using the exponential function

$$I(t) = -A(e^{-t/T_1 - \sqrt{t/c}} - d - 1)$$

where all terms retain their original definitions, and c is a spectral diffusion parameter.³ Use of one function over another did not appreciably change the T_1 values extracted, a fact reflected in the direct comparison of the monoexponential T_1 values to the T_1 values extracted using the function including a spectral diffusion term. Both sets of fitting parameters are included in Tables S2-9 and are plotted in Figure S6.

We simulated the temperature dependence of T_1 using MatLab R2017b. The function utilised was

$$\log\left(\frac{1}{T_1}\right) = \log\left(A_{dir}T + A_{ram}\left(\frac{T}{\theta_D}\right)^9 J_8\left(\frac{\theta_D}{T}\right) + A_{loc}\frac{e^{\Delta_{loc}/T}}{(e^{\Delta_{loc}/T} - 1)^2}\right)$$

where A corresponds to the coefficients associated with the direct process (*dir*), Raman process (*ram*), and local mode contributions (*loc*) respectively, θ_D is the Debye temperature, and Δ_{loc} is the energy (in K) of the local mode vibrations. J_8 is the transport integral

$$J_8\left(\frac{\theta_D}{T}\right) = \int_0^{\theta_D/T} x^8 \frac{e^x}{(e^x - 1)^2} dx$$

which can be expressed in the form of MatLab code as

```
function y = J8(x)
y = real(-(x.^8./(-1+exp(x)))+8.*(-(x.^8./8)+x.^7.* ...
log(1-exp(x))+7.*x.^6.*polylog(2,exp(x))-42.*x.^5.* ...
polylog(3,exp(x))+210.*x.^4.*polylog(4,exp(x))-840.* ...
x.^3.*polylog(5,exp(x))+2520.*x.^2.*polylog(6,exp(x))-5040.* ...
x.*polylog(7,exp(x))+5040.*polylog(8,exp(x)))-8.*(5040.* ...
polylog(8,1)));
end
```

We utilised this function rather than the function $\frac{1}{T_1} = A_{dir}T + A_{ram}\left(\frac{T}{\theta_D}\right)^9 J_8\left(\frac{\theta_D}{T}\right) + A_{loc}\frac{e^{\Delta_{loc}/T}}{(e^{\Delta_{loc}/T} - 1)^2}$ to avoid overweighting the high-temperature data.⁴ See Tables S10-11 for detailed fit parameters.

As with the T_1 data, we collected T_2 data on the highest-intensity central resonance. We utilised a Hahn echo sequence ($\pi/2 - \tau - \pi - \tau - \text{echo}$) with a 4-step phase cycle, in which $\pi/2 = 16$ ns, $\pi = 32$ ns, and τ was varied from 80 ns for each complex. We set the acquisition trigger to capture the top one-third of the spin echo, and then integrated the acquired portion of the spin echo to obtain the data. We subsequently phased the data by maximizing the sum of the data points in the real component of the spectrum. Extremely deep electron spin echo envelope modulations (ESEEM) resulting from interaction of the spin with different

nitrogen centers precluded the fitting of T_2 data without substantial overparameterization. To be more specific, this deep, multifrequency modulation arose from exact cancellation at the nitrogen atoms.⁵ This arises when the hyperfine field at a quadrupolar nucleus (such as $I = 1$ for ^{14}N) cancels out the external field, resulting in quadrupole splitting in one M_S level. We did model these data to extract a ratio of the T_2 value at a given temperature to the T_2 value at 5 K, and the temperature dependence of T_2 could be observed. This was accomplished by normalizing the data at a given temperature to the data at 5 K to eliminate the ESEEM (assumed to be temperature independent) following the method outlined by Vennam *et al.*⁶ The resulting curve was fit using the exponential function

$$N(\tau) = A * e^{2\tau/T_R}$$

where N is the curve normalised to the 5 K data, A is a scale factor, τ is delay time, and T_R in this case is the ratio of T_2 at the given temperature to the T_2 at 5 K.

Brief discussion of direct process suppression: For a complex to relax through the direct process, time reversal symmetry must be violated. One way for this symmetry to break is through the interaction of the spin with a magnetic hyperfine field.⁷ The interaction between the spin and the hyperfine field in this system, however, is weak owing to the the relatively low natural abundance (~20% for Mo and ~15% for W) of the nuclear spin-active isotopes of the transition metal on which the spin is localised. This reduces the overall influence of the hyperfine field across the sample and, we hypothesise, reduces the likelihood that the spin can relax through the direct process. This manifests in the low direct process contribution to relaxation, and in turn allows for the long T_1 times observed at 5 K.

Table S1 | Fit parameters for echo-detected EPR spectra of **1** and **2** in 0.5 mM solutions of butyronitrile. The spectra are shown in Figure S1. Natural abundances of all spin-active nuclei were used to model the hyperfine interactions. Simulations of the spectra were performed using EasySpin.⁸

Complex	g_{iso}	A_{iso} (MHz)	Linewidth (FWHM) (mT)
1	1.973	103	1.5
2	1.963	185	1.7

Table S2 | T_1 fit parameters for a 0.5 mM solution of **1** in a butyronitrile glass using the fit function

$$I(t) = -A \left(e^{-t/T_1 - \sqrt{t/c}} - d - 1 \right)$$

The standard error for each fit is reported in parentheses. The inclusion of the spectral diffusion term $\sqrt{t/c}$ throughout the fitting process proved to have minimal impact on the T_1 values extracted. This is reflected in Figure S6.

Temperature (K)	A	T_1 (s)	c (s)**	d
5*	2.48(9)	1.39(7)	1000(200)	0.0005(2)
10	0.99491)	0.0550(4)	27(7)	0.0010(5)
15	0.9960(9)	0.0396(2)	100(40)	0.0018(4)
20	0.9977(8)	0.00758(4)	30(20)	0.0006(5)
30	0.9932(10)	0.00127(1)	0(10000)	0.0037(7)
40	0.994(1)	0.000484(2)	0(7E33)	0.0030(9)
50	0.986(3)	0.000244(5)	0.1(1)	0.003(2)
60	0.995(4)	0.000134(5)	0.008(3)	-0.004(4)
70	0.988(7)	0.000061(3)	0.004(3)	-0.001(6)
80	0.979(6)	0.000033(1)	0.0005(2)	0.010(6)
90	0.965(8)	0.0000174(8)	0.00022(7)	0.020(8)
100	0.94(1)	0.0000098(7)	0.0002(1)	0.04(1)
110	0.90(1)	0.0000060(4)	0.00013(9)	0.09(2)
120	0.88(3)	0.000008(1)	0.000015(7)	0.10(3)
130	0.85(3)	0.0000026(4)	0.000(2)	0.15(4)
140	0.84(5)	0.0000021(4)	0.0000(1)	0.16(6)
150	0.77(3)	0.0000013(1)	1.42E+27	0.23(4)

* The echo at 5 K did not fully recover during the experiment, meaning that the estimate for T_1 is less reliable than the ESDs from the fitting reflect. **Spectral diffusion terms could be changed over a wide range with no observable effect on the shape of the fit curve. This is reflected in the large errors associated with these values.

Table S3 | T_1 fit parameters for a 0.5 mM solution of **1** in a butyronitrile glass using the fit function

$$I(t) = -A(e^{-t/T_1} - d - 1)$$

The standard error for each fit is reported in parentheses.

Temperature (K)	A	T_1 (s)	d
5*	2.07(5)	1.05(3)	0.0016(3)
10	0.989(1)	0.0520(3)	0.0034(7)
15	0.994(1)	0.0386(1)	0.0029(4)
20	0.9963(7)	0.00745(2)	0.0017(4)
30	0.9931(8)	0.001270(4)	0.0038(5)
40	0.994(1)	0.000484(2)	0.0029(8)
50	0.981(2)	0.000233(2)	0.008(2)
60	0.980(4)	0.000116(2)	0.010(3)
70	0.971(5)	0.000053(1)	0.014(4)
80	0.945(5)	0.0000257(5)	0.043(5)
90	0.924(5)	0.0000133(3)	0.062(5)
100	0.901(6)	0.0000080(2)	0.084(7)
110	0.860(6)	0.0000050(1)	0.140(7)
120	0.78(1)	0.0000041(2)	0.23(2)
130	0.84(1)	0.00000249(9)	0.17(1)
140	0.80(1)	0.00000181(9)	0.21(2)
150	0.77(2)	0.0000013(1)	0.23(4)

* The echo at 5 K did not fully recover during the experiment, meaning that the estimate for T_1 is less reliable than the ESDs from the fitting reflect.

Table S4 | T_1 fit parameters for a 0.5 mM solution of **1** in a 40 vol% DMF/toluene glass using the fit function

$$I(t) = -A \left(e^{-t/T_1 - \sqrt{t/c}} - d - 1 \right)$$

The standard error for each fit is reported in parentheses. The inclusion of the spectral diffusion term $\sqrt{t/c}$ proved to have minimal impact on the T_1 values extracted. This is reflected in Figure S6.

Temperature (K)	A	T_1 (s)	c (s)**	d
5	0.975(5)	1.48(5)	34(8)	0.003(1)
10	0.990(3)	0.139(3)	4.7(6)	0.0060(9)
15	0.982(3)	0.0275(6)	3(1)	0.010(2)
20	0.983(3)	0.0068(1)	3(1)	0.006(2)
30	0.983(3)	0.00134(3)	0(20)	0.009(2)
40	0.988(3)	0.000492(5)	0(1E37)	0.009(2)
50	0.981(3)	0.000214(3)	0(3E35)	0.010(2)
60	0.978(4)	0.000103(1)	5 E 24	0.012(3)
70	0.979(6)	0.000051(2)	0.006(4)	0.009(5)
80	0.96(1)	0.000030(2)	0.002(3)	0.00(1)
90	0.99(1)	0.000019(1)	0.0003(2)	0.00(1)
100	0.97(2)	0.000011(1)	0.0002(2)	0.0(2)
110	0.97(2)	0.000009(1)	0.00004(2)	0.00(2)
120	0.99(2)	0.000007(1)	0.000015(5)	0.00(2)

**Spectral diffusion terms could be changed over a wide range with no observable effect on the shape of the fit curve. This is reflected in the large errors associated with these values.

Table S5 | T_1 fit parameters for a 0.5 mM solution of **1** in a 40 vol% DMF/toluene glass using the monoexponential fit function

$$I(t) = -A(e^{-t/T_1} - d - 1)$$

The standard error for each fit is reported in parentheses.

Temperature (K)	A	T_1 (s)	d
5	0.957(7)	1.13(3)	0.010(2)
10	0.964(7)	0.110(2)	0.014(2)
15	0.973(3)	0.0245(3)	0.015(2)
20	0.978(2)	0.00638(6)	0.009(1)
30	0.982(3)	0.00132(1)	0.011(2)
40	0.988(3)	0.000492(5)	0.009(2)
50	0.982(3)	0.000214(2)	0.010(1)
60	0.979(4)	0.000103(1)	0.012(3)
70	0.966(4)	0.0000552(9)	-0.021(3)
80	0.948(6)	0.0000267(7)	0.025(5)
90	0.949(7)	0.0000151(4)	0.034(6)
100	0.91(1)	0.0000091(4)	0.05(1)
110	0.90(1)	0.0000060(2)	-0.08(1)
120	0.88(1)	0.0000040(2)	0.10(1)

Table S6 | T_1 fit parameters for a 0.5 mM solution of **2** in a butyronitrile glass using the fit function

$$I(t) = -A \left(e^{-t/T_1 - \sqrt{t/c}} - d - 1 \right)$$

The standard error for each fit is reported in parentheses. The inclusion of the spectral diffusion term $\sqrt{t/c}$ proved to have minimal impact on the T_1 values extracted. This is reflected in Figure S6.

Temperature (K)	A	T_1 (s)	c (s)*	d
5	0.95(1)	1.8(4)	1.9(4)	0.000(5)
10	0.989(2)	0.0713(5)	22(4)	0.0009(5)
15	0.991(1)	0.0120(1)	12(5)	0.0012(8)
20	0.993(2)	0.00133(2)	6(10)	-0.002(1)
30	0.988(4)	0.00030(1)	0.02(1)	-0.000(3)
40	0.989(5)	0.000095(3)	0.006(2)	0.000(3)
50	0.973(8)	0.000027(1)	0.003(2)	-0.015(6)
60	0.939(6)	0.0000100(3)	0.0006(2)	0.060(6)
70	0.888(9)	0.0000043(2)	0.00017(9)	-0.12(1)
80	0.79(2)	0.0000020(2)	0.00004(3)	-0.26(3)
90	0.83(3)	0.0000021(3)	0.0000018(5)	-0.19(4)

*Spectral diffusion terms could be changed over a wide range with no observable effect on the shape of the fit curve. This is reflected in the large errors associated with these values.

Table S7 | T_1 fit parameters for a 0.5 mM solution of **2** in a butyronitrile glass using the fit function

$$I(t) = -A(e^{-t/T_1} - d - 1)$$

The standard error for each fit is reported in parentheses.

Temperature (K)	A	T_1 (s)	d
5	1.0	0.63(5)	0.003(9)
10	0.991(2)	0.0664(5)	0.0038(8)
15	0.988(2)	0.01157(7)	0.0031(7)
20	0.991(2)	0.001310(8)	0.0034(9)
30	0.975(4)	0.000268(4)	0.011(3)
40	0.973(4)	0.000083(1)	0.015(3)
50	0.965(5)	0.0000249(4)	0.029(3)
60	0.912(4)	0.0000087(1)	-0.084(3)
70	0.858(4)	0.00000371(6)	0.160(5)
80	0.742(6)	0.00000167(4)	0.330(9)
90	0.66(1)	0.00000097(4)	0.48(2)

Table S8 | T_1 fit parameters for a 0.5 mM solution of **2** in a 40 vol% DMF/toluene glass using the fit function

$$I(t) = -A \left(e^{-t/T_1 - \sqrt{t/c}} - d - 1 \right)$$

The standard error for each fit is reported in parentheses. The inclusion of the spectral diffusion term $\sqrt{t/c}$ proved to have minimal impact on the T_1 values extracted. This is reflected in Figure S6.

Temperature (K)	A	T_1 (s)	c (s)*	d
5	0.989(3)	0.469(9)	21(3)	0.002(1)
10	0.991(3)	0.0304(7)	1.5(3)	0.003(1)
15	0.984(2)	0.00393(8)	1×10^3 (2)	0.005(2)
20	0.971(3)	0.00131(1)	-3×10^{33} (0)	-0.011(2)
30	0.95(1)	0.00031(3)	0.011(8)	-0.022(9)
40	0.930(5)	0.000062(1)	-3×10^{25} (0)	-0.057(4)
50	0.859(9)	0.0000215(6)	9×10^{26} (0)	0.115(6)
60	0.77(1)	0.0000075(2)	8×10^{25} (0)	0.242(8)
70	0.64(1)	0.0000029(1)	2×10^{24} (0)	0.52(2)
80	0.50(1)	0.0000018(1)	2×10^{30} (0)	0.95(4)
90	0.40(2)	0.0000009(1)	-1×10^{29} (3)	1.4(1)

*Spectral diffusion terms could be changed over a wide range with no observable effect on the shape of the fit curve. This is reflected in the large errors associated with these values.

Table S9 | T_1 fit parameters for a 0.5 mM solution of **2** in a 40 vol% DMF/toluene glass using the fit function.

$$I(t) = -A(e^{-t/T_1} - d - 1)$$

The standard error for each fit is reported in parentheses.

Temperature (K)	A	T_1 (s)	d
5	0.973(5)	0.388(6)	0.008(2)
10	0.978(5)	0.0255(4)	0.011(2)
15	0.983(2)	0.00392(4)	0.006(1)
20	0.971(3)	0.00131(1)	0.012(2)
30	0.929(8)	0.000256(9)	0.038(6)
40	0.930(5)	0.000062(1)	0.057(4)
50	0.882(7)	0.0000218(6)	0.115(6)
60	0.796(6)	0.0000076(2)	0.241(7)
70	0.650(9)	0.0000031(1)	0.51(2)
80	0.50(2)	0.0000018(1)	0.95(4)
90	0.41(2)	0.0000009(1)	1.4(1)

Table S10 | Parameters from fitting the temperature dependence of T_1 using the fit function

$$\log\left(\frac{1}{T_1}\right) = \log\left(A_{dir}T + A_{ram}\left(\frac{T}{\theta_D}\right)^9 J_8\left(\frac{\theta_D}{T}\right) + A_{loc}\frac{e^{\Delta_{loc}/T}}{(e^{\Delta_{loc}/T} - 1)^2}\right)$$

while using T_1 values extracted using the fit function including a spectral diffusion term

$$I(t) = -A\left(e^{-t/T_1 - \sqrt{t/c}} - d - 1\right)$$

Errors from fitting are presented as 95% confidence bounds.

Sample	A_{dir} ($s^{-1} K^{-1}$)	A_{loc} ($s^{-1} \times 10^8$)	A_{ram} ($s^{-1} \times 10^5$)	Δ_{loc} (K)	θ_D (K)
1 (0.5 mM in PrCN)	0.149 (-0.001, 0.299)	0.129 (-0.066, 0.325)	0.462 (-0.171, 1.095)	494.1 (338.1, 649.8)	76.73 (49.2, 104.3)
2 (0.5 mM in PrCN)	0.107 (0.02353, 0.1905)	0.2407 (-0.2037, 0.6851)	4.318 (-2.376, 11.01)	339.6 (213.1, 466.1)	102.1 (73.03, 131.2)
1 (0.5 mM in DMF/Tol)	0.138 (0.08674, 0.1893)	0.072 (0.0022, 0.141)	0.67 (0.215, 1.12)	350 (279.1, 420.8)	88.32 (74.99, 101.7)
2 (0.5 mM in DMF/Tol)	0.3986 (0.2934, 0.5038)	0.3911 (-0.1933, 0.589)	2.039 (0.9617, 3.11)	339.8 (306.9, 372.6)	78.36 (69.13, 87.58)

Table S11 | Parameters from fitting the temperature dependence of T_1 using the fit function

$$\log\left(\frac{1}{T_1}\right) = \log\left(A_{dir}T + A_{ram}\left(\frac{T}{\theta_D}\right)^9 J_8\left(\frac{\theta_D}{T}\right) + A_{loc}\frac{e^{\Delta_{loc}/T}}{(e^{\Delta_{loc}/T} - 1)^2}\right)$$

while using T_1 values extracted using the fit function

$$I(t) = -A(e^{-t/T_1} - d - 1)$$

Errors from fitting are presented as 95% confidence bounds.

Sample	A_{dir} ($s^{-1} K^{-1}$)	A_{local} ($s^{-1} \times 10^8$)	A_{ram} ($s^{-1} \times 10^5$)	Δ_{loc} (K)	θ_D (K)
1 (0.5 mM in PrCN)	0.213 (0.027, 0.399)	0.2 (-0.06, 0.46)	0.53(-0.12, 0.12)	514 (380.2, 648.2)	79.5 (53.8, 105)
2 (0.5 mM in PrCN)	0.3428 (0.1367, 0.549)	0.9424 (-.7458, 2.631)	8.569 (-1.679, 18.82)	416.1 (287, 545.3)	115.8 (89.91, 141.6)
1 (0.5 mM in DMF/Tol)	0.209 (0.120, 0.300)	0.072 (0.0022, 0.141)	0.67 (0.21, 1.15)	432.5 (345.1, 519.8)	85.6 (71.2, 100)
2 (0.5 mM in DMF/Tol)	0.4915 (0.3102, 0.6728)	0.4349 (0.1038, 0.7649)	2.353 (0.6501, 4.056)	350 (299.6, 400.4)	79.23 (66.38, 92.07)

Table S12 | Temperature dependence of T_2 for a 0.5 mM solution of **1** in butyronitrile relative to the T_2 at 5 K extracted using the equation

$$N(\tau) = A * e^{2\tau/T_R}$$

These data are plotted in Figure S9.

Temperature (K)	Change in T_2 ratio (T_R) (compared to 5K T_2)	A
10	0.0000190	1.0192
20	-0.000217	0.9564
30	0.0000860	1.0184
40	0.0001170	1.0245
50	0.0001360	1.0248
60	0.0001120	1.0253
70	-0.0000157	0.9821
80	-0.0000703	0.9677
90	0.0002010	1.0758
100	0.0011300	1.3392
110	0.0026500	1.9293
120	0.0050700	3.3190
130	0.0081000	6.6383
140	0.0098000	9.6361
150	0.0112000	13.0688

Table S13 | Temperature dependence of T_2 for a 0.5 mM solution of **1** in 40 vol% DMF/toluene relative to the T_2 at 5 K extracted using the equation

$$N(\tau) = A * e^{2\tau/T_R}$$

These data are plotted in Figure S9.

Temperature (K)	Change in T_2 ratio (T_R) (compared to 5K T_2)	A
10	0.000501	1.0122
15	0.000696	1.0179
20	0.000772	1.0128
30	0.000148	1.0438
40	0.000183	1.0401
50	0.000301	1.0739
60	0.000738	1.1939
70	0.000651	1.1779
80	0.000324	1.0963
90	0.000217	1.0529
100	0.000129	1.0587
110	0.000108	1.0439
120	0.000292	1.0808

Table S14 | Temperature dependence of T_2 for a 0.5 mM solution of **2** in butyronitrile relative to the T_2 at 5 K extracted using the equation

$$N(\tau) = A * e^{2\tau/T_R}$$

These data are plotted in Figure S10.

Temperature (K)	Change in T_2 ratio (T_R) (compared to 5K T_2)	A
10	0.000117	1.0478
15	0.000136	1.0432
20	0.000112	1.0455
30	-0.0000157	1.0528
40	-0.0000703	1.0480
50	0.000201	1.0825
60	0.00113	1.0963
70	0.00265	1.1779
80	0.00507	1.4256
90	0.00810	1.8171

Table S15 | Temperature dependence of T_2 for a 0.5 mM solution of **2** in 40 vol% DMF/toluene relative to the T_2 at 5 K using the equation

$$N(\tau) = A * e^{2\tau/T_R}$$

These data are plotted in Figure S10.

Temperature (K)	Change in T_2 ratio (T_R) (compared to 5K T_2)	A
10	0.0000809	1.0053
15	0.000116	1.0161
20	0.000167	1.0186
30	0.000200	1.0365
40	0.000258	1.0281
50	0.00116	1.2502
60	0.00221	1.5453
70	0.00244	1.6784
80	0.00334	1.9737
90	0.00360	1.9010

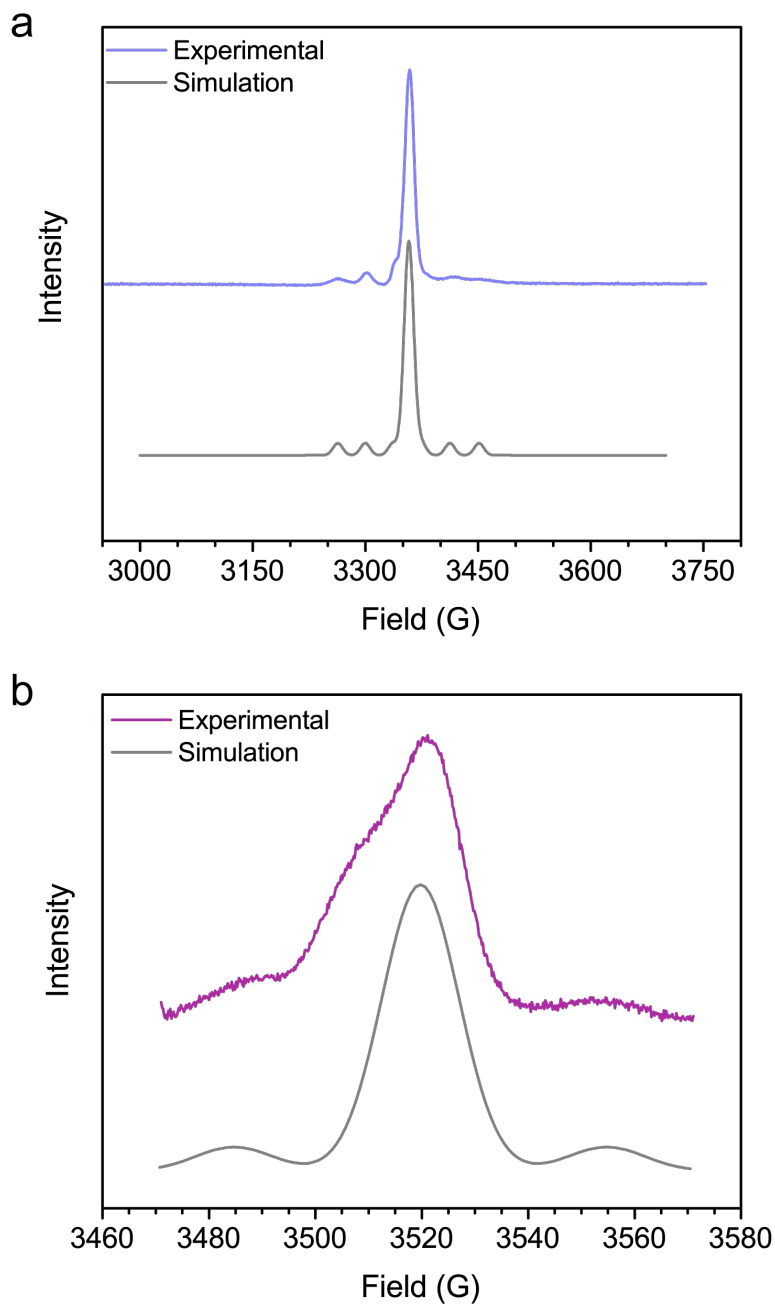


Figure S1 | Echo-detected EPR spectrum of (a) **1** and (b) **2** in a 0.5 mM butyronitrile glass at 20 K. T_1 and T_2 data were collected at the highest central resonance at approximately 3370 G (**1**) and 3520 G (**2**). Fit parameters can be found in Table S1.

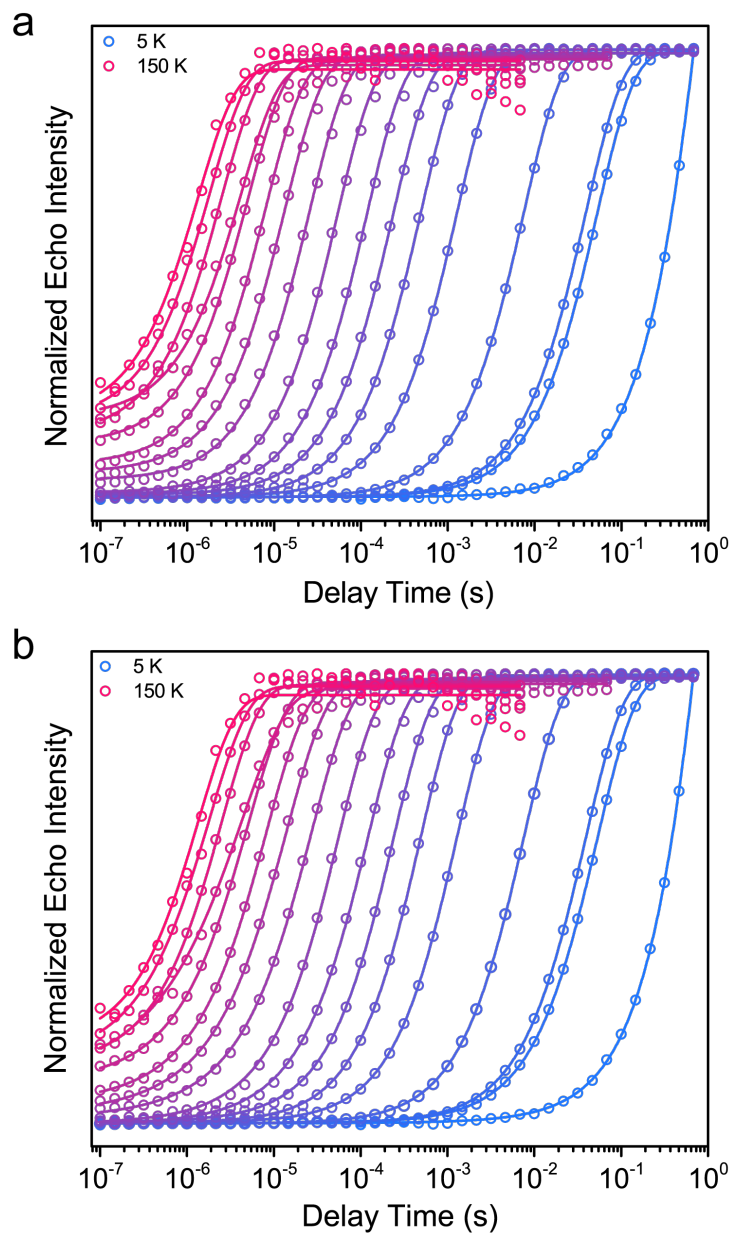


Figure S2 | Saturation recovery curves collected on a 0.5 mM solution of **1** in butyronitrile. Solid lines are fits to the data using an (a) monoexponential function, and (b) a function incorporating a term including spectral diffusion. As was noted earlier, using one fit over another did not appreciably change T_1 values extracted.

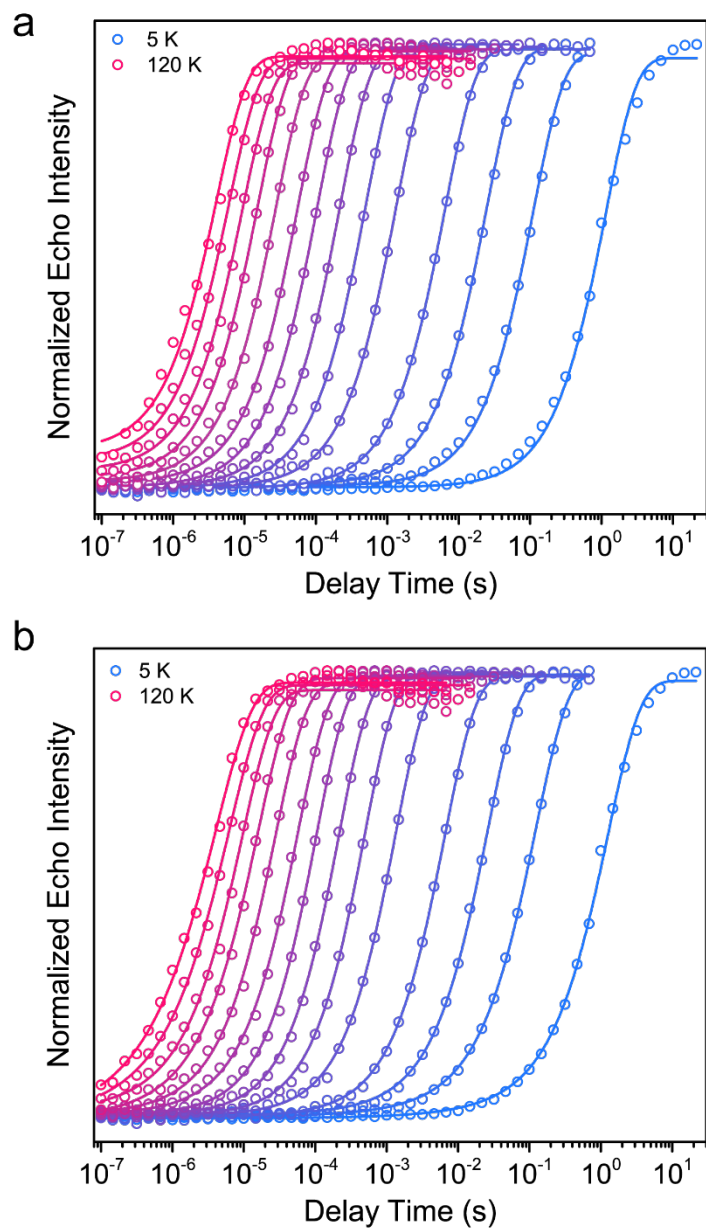


Figure S3 | Saturation recovery curves collected on a 0.5 mM solution of **1** in 40 vol% DMF/toluene. Solid lines are fits to the data using an (a) monoexponential function, and (b) a function incorporating a term including spectral diffusion. As was noted earlier, using one fit over another did not appreciably change T_1 values extracted.

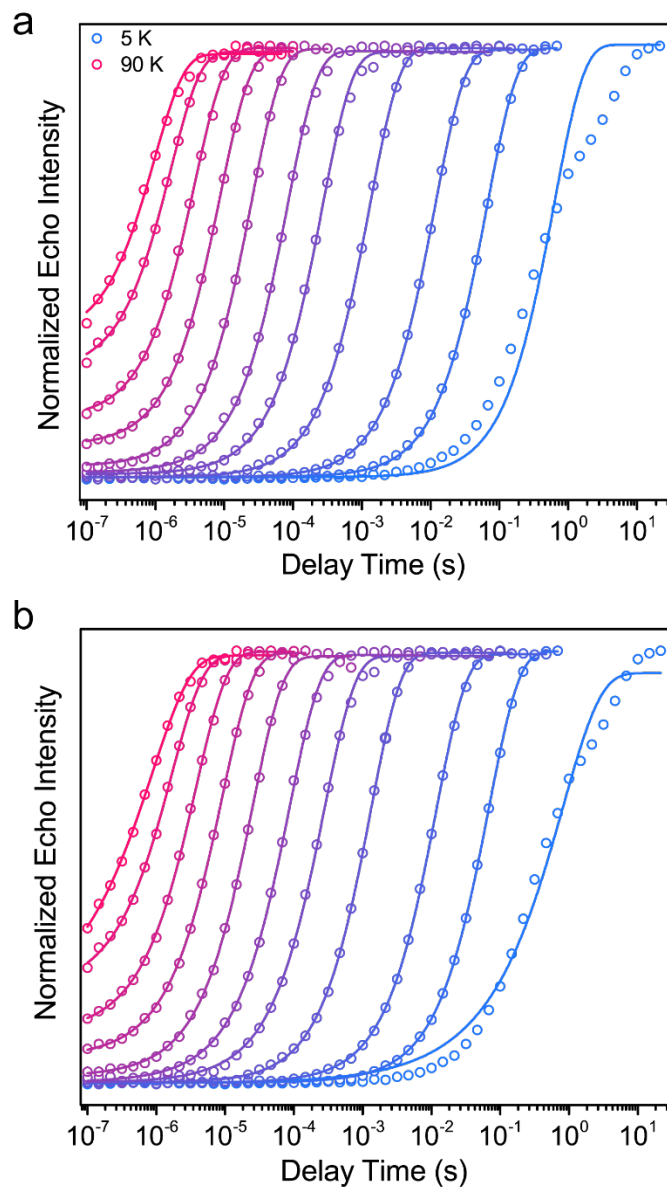


Figure S4 | Saturation recovery curves collected on a 0.5 mM solution of **2** in butyronitrile. Solid lines are fits to the data using an (a) monoexponential function, and (b) a function incorporating a term including spectral diffusion. As was noted earlier, using one fit over another did not appreciably change T_1 values extracted.

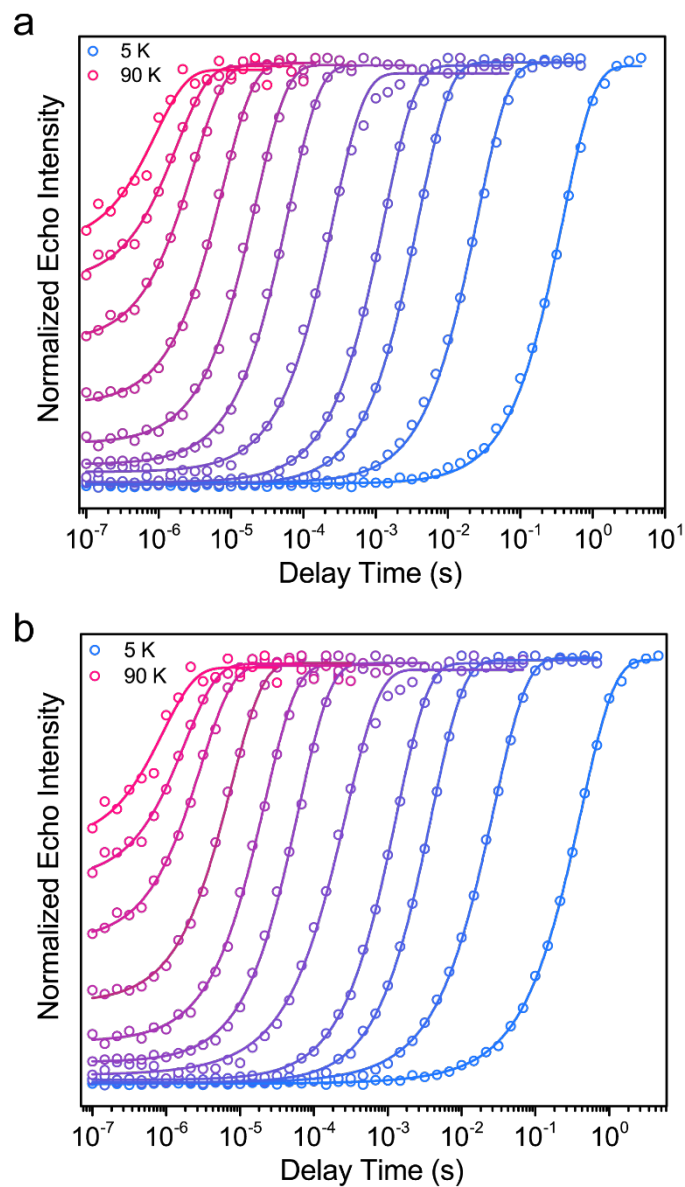


Figure S5 | Saturation recovery curves collected on a 0.5 mM solution of **2** in 40 vol% DMF/toluene. Solid lines are fits to the data using an (a) monoexponential function, and (b) a function incorporating a term including spectral diffusion. As was noted earlier, using one fit over another did not appreciably change T_1 values extracted.

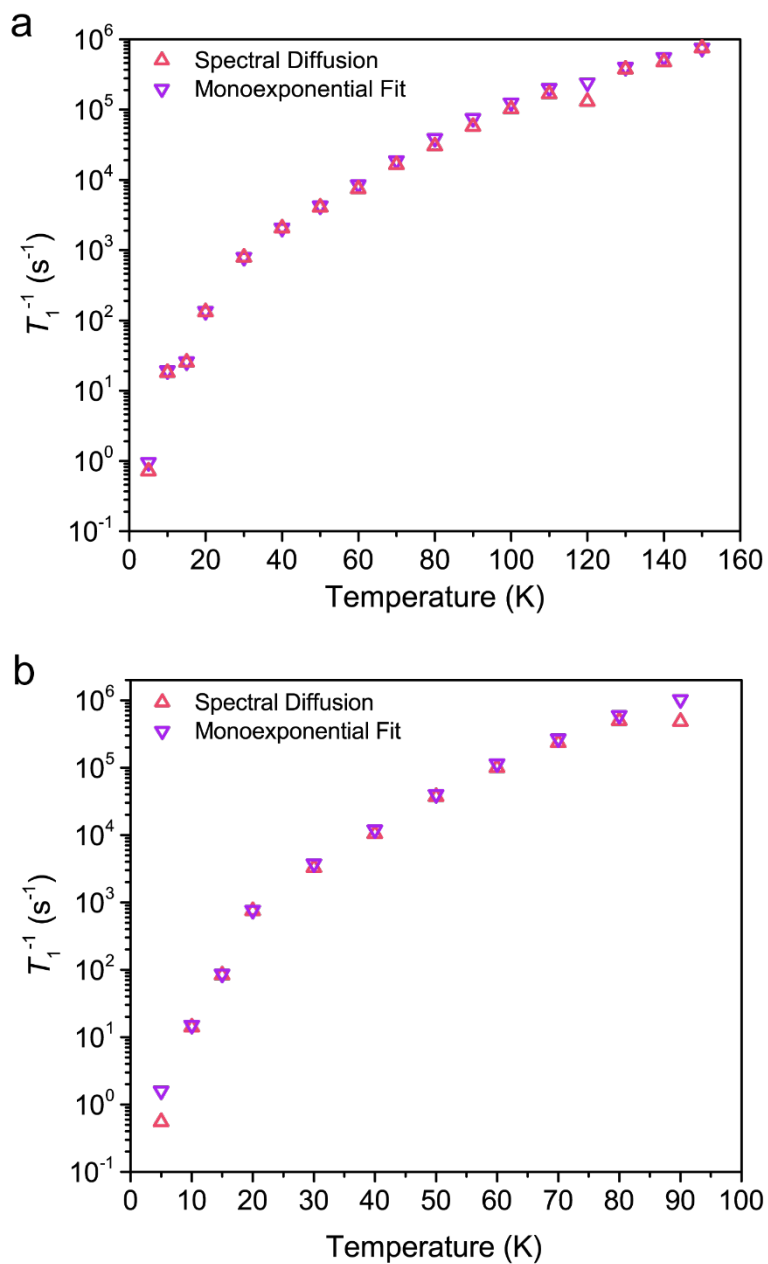


Figure S6 | Comparison of T_1 values of **1** (0.5 mM) and **2** (0.5 mM) in butyronitrile extracted using a monoexponential fit vs. using a fit including a spectral diffusion term for (a) $[\text{Mo}(\text{CN})_8]^{3-}$ and (b) $[\text{W}(\text{CN})_8]^{3-}$. The T_1 values only diverge slightly and remain within experimental error, so spectral diffusion was determined to have a minimal influence on T_1 . This is expected for data collected through a saturation recovery experiment.

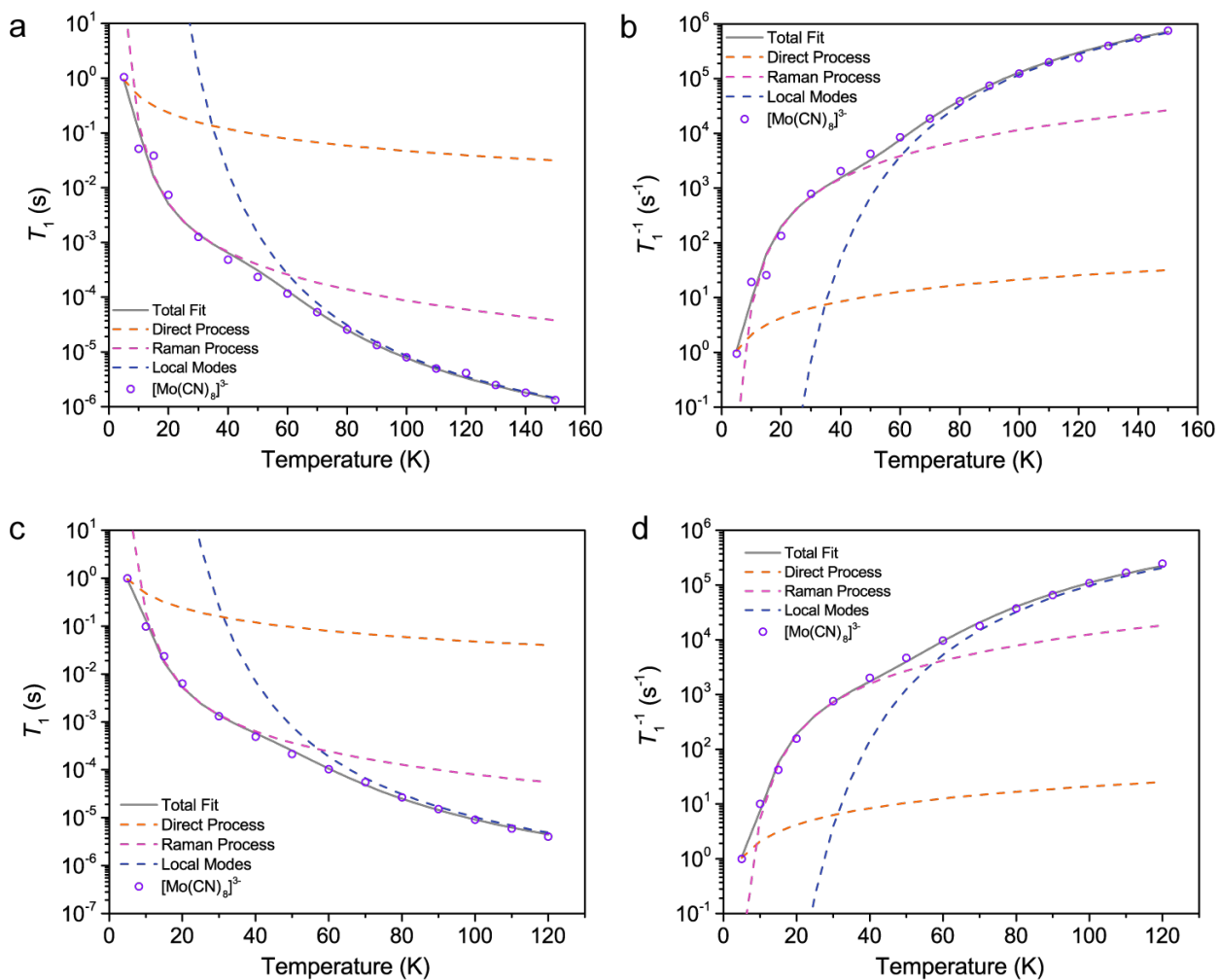


Figure S7 | Temperature dependence of T_1 for 0.5 mM solutions of **1** in (a,b) PrCN and (c,d) 40 vol% DMF/toluene. T_1 values were extracted using a monoexponential function. We also included the same data plotted as the rate of relaxation (T_1^{-1}) (b, d). Fit parameters are included in Tables S10 and S11.

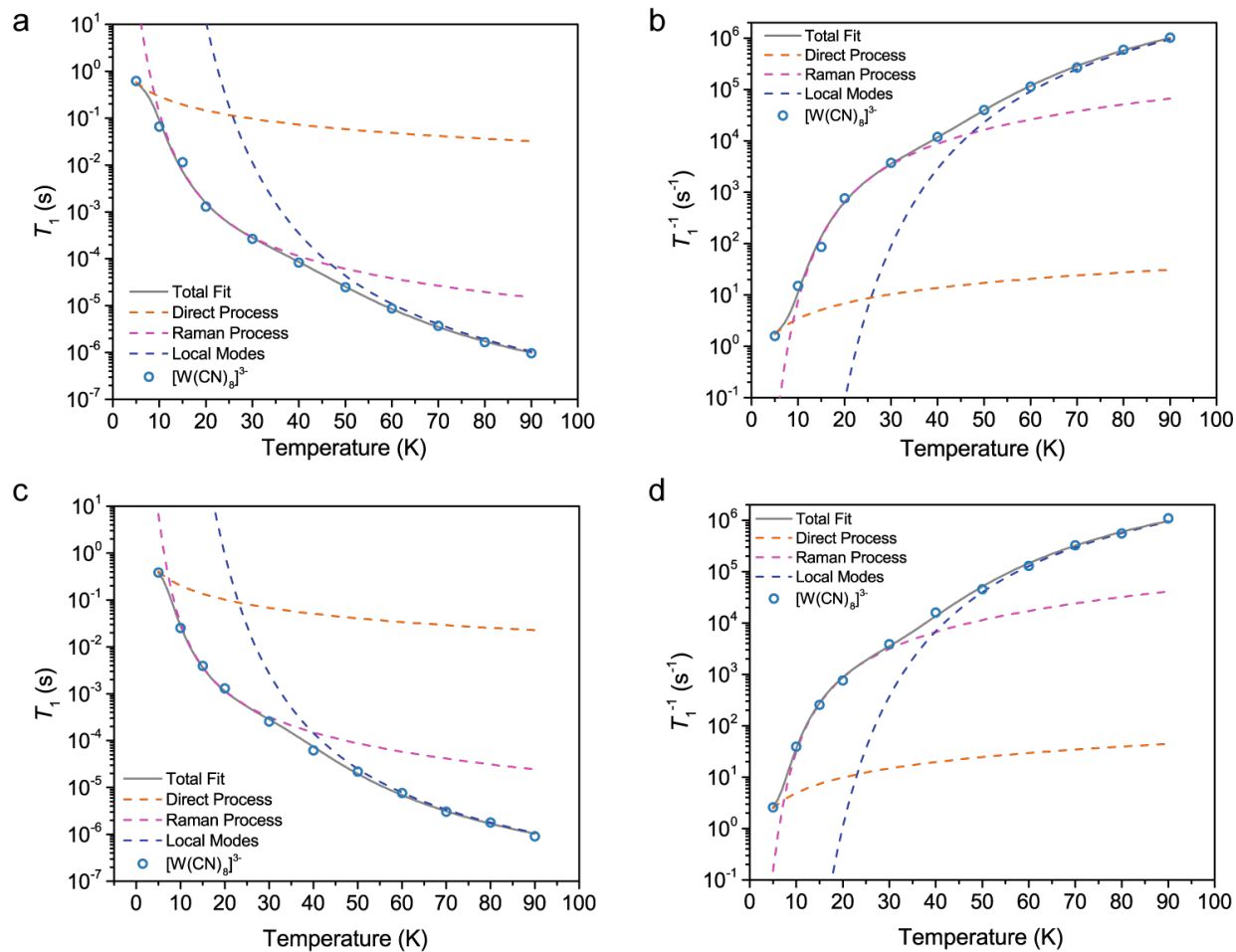


Figure S8 | Temperature dependence of T_1 for 0.5 mM solutions of **2** in (a,b) PrCN and (c,d) 40 vol% DMF/toluene. T_1 values were extracted using a monoexponential function. We also included the same data plotted as the rate of relaxation (T_1^{-1}) (b, d). Fit parameters are included in Tables S10 and S11.

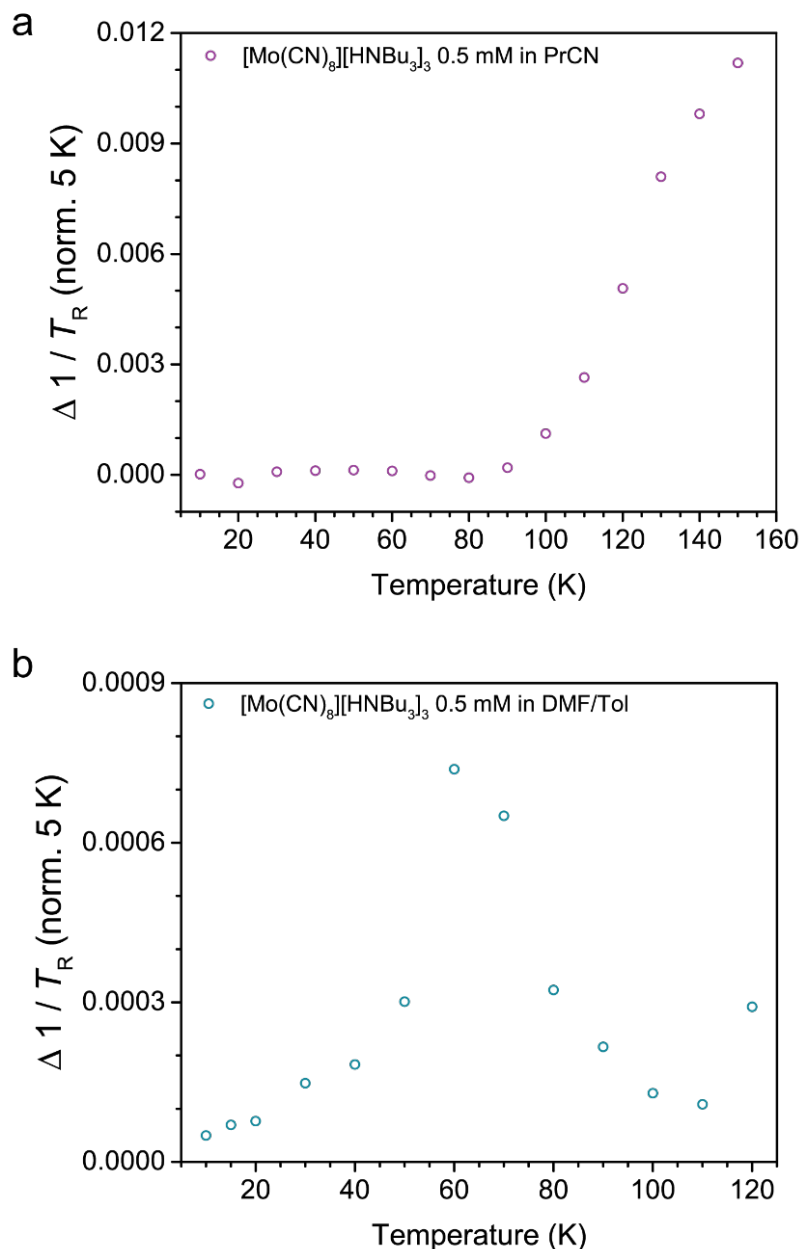


Figure S9 | Temperature dependence of T_2 normalised to the T_2 value at 5 K for 0.5 mM solutions of **1** in a) butyronitrile, and b) 40 vol% DMF/toluene. As temperature increases, the spin-spin relaxation rate generally increases. This trend is commensurate with T_2 studies on other transition metal systems. Absolute values of T_2 could not be determined at X-band because of exact cancellation, but the temperature dependence was determined *via* normalization of the data to the 5 K decay curve to remove ESEEM modulation and extraction of relative T_2 from the resulting normalised decay curve.

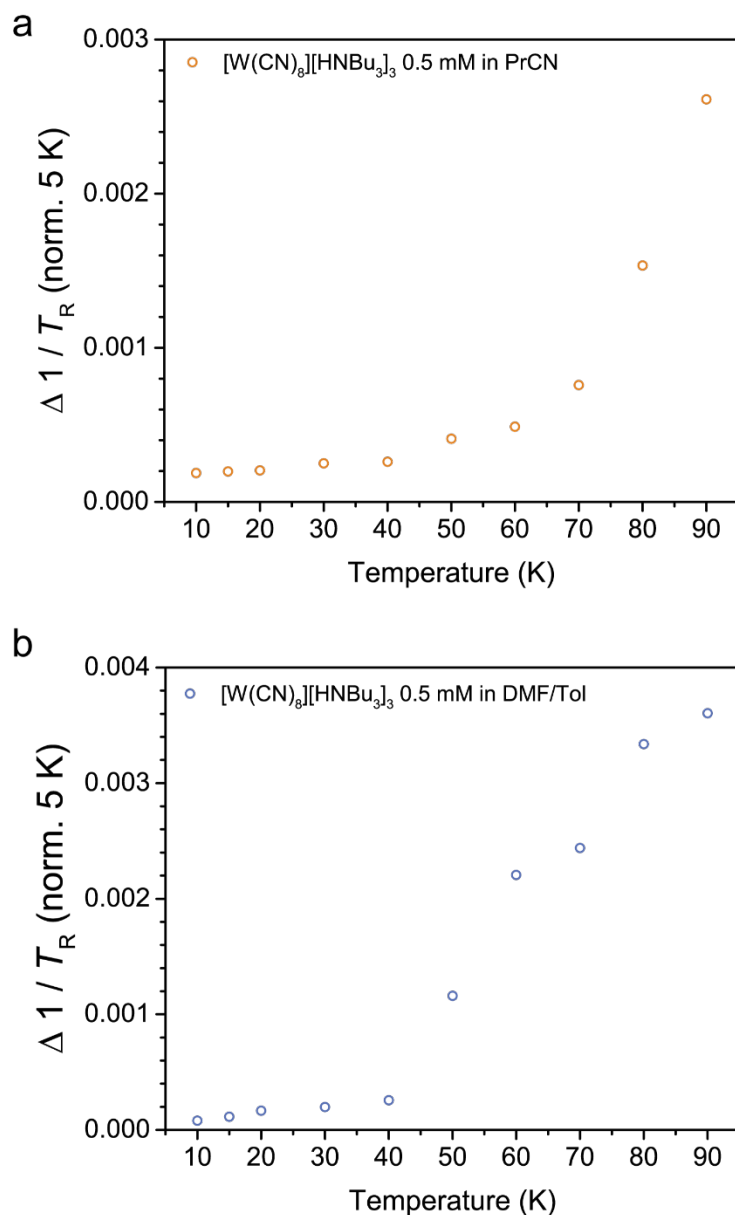


Figure S10 | Temperature dependence of T_2 normalised to the T_2 value at 5 K for 0.5 mM solutions of **2** in (a) butyronitrile, and (b) 40 vol% DMF/toluene. As temperature increases, the spin-spin relaxation rate generally increases. This trend is commensurate with T_2 studies on other transition metal systems. Absolute values of T_2 could not be determined at X-band because of exact cancellation, but the temperature dependence was determined *via* normalization of the data to the 5 K decay curve to remove ESEEM modulation and extraction of relative T_2 from the resulting normalised decay curve.

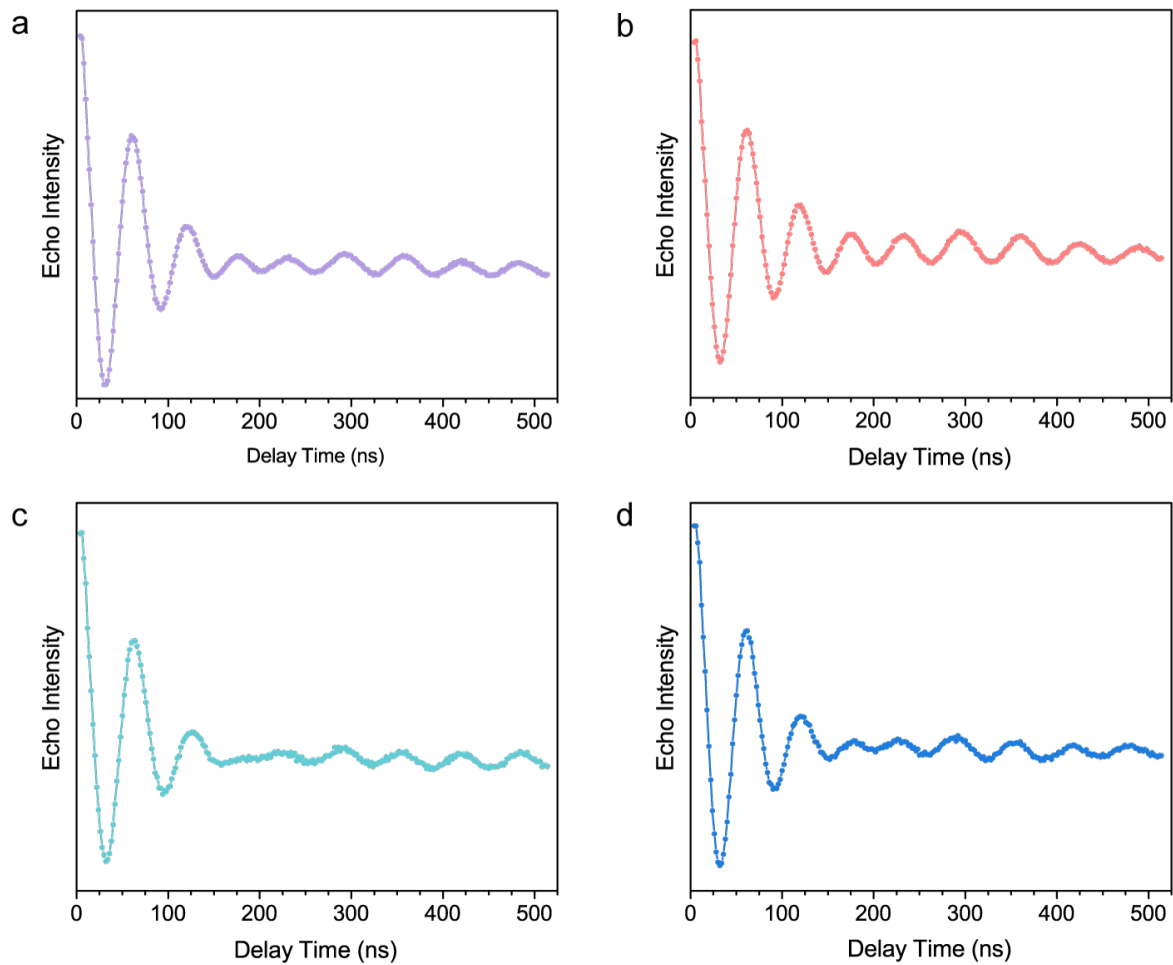


Figure S11 | Nutation data for **1** (a)(b), and **2** (c)(d), as 0.5 mM solutions in PrCN (a)(c), and 40 vol% DMF/toluene (b)(d) collected at 20 K. Solid line is a guide for the eyes.

References

- (1) L. Bok, J. Leipoldt and S. Basson, *Z. Anorg. Allg. Chem.*, 1975, **415**, 81–83.
- (2) J. M. Zadrozny, J. Niklas, O. G. Poluektov and D. E. Freedman, *ACS Cent. Sci.*, 2015, **1**, 488–492.
- (3) H. Chen, A. G. Maryasov, O. Y. Rogozhnikova, D. V. Trukhin, V. M. Tormyshev and M. K. Bowman, *Phys. Chem. Chem. Phys.*, 2016, **18**, 24954–24965.
- (4) L. J. Berliner, S. S. Eaton and G R. Eaton, *Biological Magnetic Resonance: Distance Measurements in Biological Systems by EPR*, vol. 19, Kluwer Academic/Plenum Publishers: New York, 2000.
- (5) H. L. Flanagan and D. J. Singel, *J. Chem. Phys.*, 1987, **87**, 5606–5616.
- (6) P. R. Vennam, N. Fisher, M. D. Krzyaniak, D. M. Kramer and M. K. Bowman, *ChemBioChem*, 2013, **14**, 1745–1753.
- (7) A. Abragam and B. Bleaney, *Electron paramagnetic resonance of transition ions*, Clarendon Press, Oxford, 1970.
- (8) S. Stoll, A. Schweiger *EasySpin, a comprehensive software package for spectral simulation and analysis in EPR*, *J. Magn. Reson.* 2006, **178**(1), 42-55.